

Broadband noise filtering in random sequences of coherent pulses using the temporal Talbot effect

Carlos R. Fernández-Pousa and Felipe Mateos

División de Óptica, Departamento de Ciencia y Tecnología de Materiales, Universidad Miguel Hernández, Avenida Ferrocarril s/n, E03202 Elche (Alicante) Spain

Laura Chantada, María Teresa Flores-Arias, Carmen Bao, María Victoria Pérez, and Carlos Gómez-Reino

Grupo de Óptica GRIN, Departamento de Física Aplicada, Universidade de Santiago de Compostela, Campus Sur, E15782 Santiago de Compostela, Spain

Received August 27, 2003; revised manuscript received December 9, 2003; accepted January 6, 2004

The exact power spectrum of the detected optical envelope of a train of random pulses after the temporal Talbot effect is computed. The input train into a Talbot device consists of a sequence of chirped Gaussian pulses whose appearance in the train is probabilistic. Dispersion provides a Talbot replica of the original train. The resulting noise spectrum shows narrow spectral windows below a broadband output noise envelope. The noise-envelope width depends on the value of the chirp, coinciding with the single-pulse spectrum only if the pulses are unchirped. The locations and width of the spectral windows depend on the values of the chirp and the temporal width of the pulses in the train. For wide pulses, high output harmonics, and low dispersive devices, these windows are cosine-squared modulated. The properties of this modulation depend only on the statistics of the appearance of the pulses. © 2004 Optical Society of America

OCIS codes: 030.1670, 060.2340, 070.6760, 320.5550.

1. INTRODUCTION

The temporal Talbot effect¹ is a coherent phenomenon that consists of the repetition of a pulse train after its linear propagation along a highly dispersive line. Although it has been demonstrated using high-dispersion fiber,²⁻⁴ linearly chirped fiber gratings⁵ (LCFGs) are the preferred dispersive media, since they represent flexible devices where practical requirements such as the high dispersion and spectral width of the filter can be chosen independently. After the proposal⁵ of the use of the fractional Talbot effect as a tool to generate high-frequency trains of pulses, several groups have reported on demonstrations of Talbot devices using LCFGs, with both amplitude⁶ and phase⁷ modulation. The flexibility of design of LCFGs has permitted the simultaneous performance of other all-optical tasks, such as compression⁷ or reshaping.⁸ With superimposed LCFGs, trains of 100 GHz have been generated.⁹ In other research studies, Talbot repetition rates have been shown using joint designs of Talbot filters, based on high-dispersion fiber, with other active devices, such as Raman compressors¹⁰ or semiconductor optical amplifiers.¹¹ Finally, operation of fiber lasers based on this effect has also been reported, both in integer Talbot¹² and in fractional Talbot regimes.¹³ In all these demonstrations, the pulse trains range in the microwave or millimeter-wave spectrum, between 10 and 400 GHz.

However, little attention has been paid to these devices as smoothers of imperfections in the original train. This capability is, however, well known in diffractive

optics.^{14,15} Recently,¹⁶ we have shown how the Talbot effect smooths the imperfections due to mistiming of the pulses in the train in the temporal domain. Studies on imperfections of the Talbot-imagined trains have also been reported,¹⁷ however, our approach is purely stochastic and aimed at the description of the spectrum of the detected envelope.

The main motivation of our study is the description, in a concrete model, of the spectral content of a nonideal Talbot-imagined coherent train of pulses. To the best of our knowledge, this is the first report on this topic in the context of both the spatial and the temporal Talbot effect. Among the possible deviations of nonideality, here we will focus in the randomly on-off keying of the pulses of the train. We will refer to the result of a Talbot-imagined random train of pulses as the random Talbot effect. The assumptions of Gaussian and chirped pulses, together with the independence of the variables describing the presence or absence of the train, allow an exact stochastic characterization of the microwave spectrum.

The main outcomes of our results are the following: noise is peaked around concrete locations of the spectrum, and each of these peaks can show a cosine-squared modulation. The centers of the peaks are shifted depending on the value of the chirp. This allows an indirect characterization of the pulses in the train through the analysis of the spectrum. In particular, measurement of the positions and the width of the peaks results in the determination of the chirp of the initial pulses. Moreover, the re-

sulting noise spectrum varies continuously with respect to the parameters that define the model. This means that, in order to observe the spectral features of noise, no fine tuning of the initial repetition rate of the train is necessary to match the Talbot conditions, in contrast with the temporal domain,⁶ where the trace of the Talbot effect is the increase of the repetition rate of the train. However, for clarity, our results are derived under the assumption of exact Talbot conditions.

This paper is organized as follows. In Section 2, we compute the exact power spectrum of the random Talbot effect. The main features of the spectrum are presented in this section. We also introduce a useful approximation of the power spectrum, used in the following. Our first part of the analysis, Section 3, deals with the simplest case where the cosine-squared modulation can be neglected and shows the influence of the chirp in the spectrum. In Section 4, we analyze the modulation. Finally, we conclude with Section 5.

2. COMPUTATION OF THE POWER SPECTRUM

Pulse propagation in a dispersive linear medium with negligible attenuation can be described as follows. Let us consider a dispersive medium where a monochromatic wave of frequency ω_0 is modulated by a complex pulse envelope $x(z, t)$. The basic equation governing its propagation along a distance z is^{18,19}

$$\frac{\partial x}{\partial z} = -i \frac{\beta_2}{2} \frac{\partial^2 x}{\partial t^2}, \quad (1)$$

where $\beta(\omega) = \beta_0 + (\omega - \omega_0)\beta_1 + (\omega - \omega_0)^2\beta_2/2 + \dots$ is the expansion of the dispersion relation about the carrier frequency and t is the time measured in the proper reference frame of the pulse, $t = t_{\text{phy}} - \beta_1 z$, with t_{phy} being the physical time. β_3 and other higher-order dispersion terms will not be taken into account. Then, Eq. (1) is formally equivalent to the equation describing paraxial diffraction in one dimension, and the corresponding analogy is the basis for space-time duality between one-dimensional paraxial diffraction and pulse propagation in dispersive media.

The propagator associated with the dispersion equation (1) is the Fresnel propagator:

$$h_\xi(t - t') = (-2\pi i \xi)^{-1/2} \exp[-i(t - t')^2/2\xi], \quad (2)$$

where the parameter ξ accounts for the total dispersion of the device. For instance, for a system with length L and first-order dispersion coefficient β_2 , $\xi = \beta_2 L$. The temporal Talbot effect arises when a train of period t_0 is introduced in a dispersive medium of this type. The absolute value of the total dispersion ξ is to be related to the period of the incoming train as $|\xi| = t_0^2 \gamma / 2\pi \alpha$, where α and γ are positive and coprime integers. Then the total dispersion is a fraction of a basic dispersion scale, $t_0^2/2\pi$. For typical applications in the microwave regime, the incoming train has a frequency in the range 1–10 GHz, so that this dispersion scale lies in the range 10^3 – 10^5 ps²/rad.

When $\alpha = 1$, the effect is called the integer Talbot, and the output train is a replica of the incoming train shifted by half a time slot if γ is odd. If $\alpha \neq 1$, the effect is called the fractional Talbot. The output train in this case has a richer structure. It is again a periodic train of pulses with period t_0 , shifted for odd γ . But the unit interval is composed by the coherent sum of α replicas of the original pulse, shifted mutually by t_0/α , with power reduced by $1/\alpha$ and with definite phase differences between them. Repetition rates of the original train of pulses with rate $N\times$ can be obtained from $\gamma/\alpha = 1/N$ if the initial pulses are short enough to avoid superposition of neighboring pulses in each time slot. In general, a dispersive device adjusted to a certain Talbot index γ/α will produce an increase by $\alpha\times$ of the repetition rate. We will use the notations $\omega_f = 2\pi/t_0$ and $\alpha\omega_f$ for the fundamental harmonics of the input and the output trains, respectively.

We are interested in the behavior of this device when it is fed with a coherent train composed of randomly distributed pulses. The pulse envelope will be assumed linearly chirped Gaussian:

$$\begin{aligned} x_0(t) &= \sum_k b_k f(t - kt_0) \\ &= \sum_k b_k \exp[-(t - kt_0)^2(1 + iC)/2t_p^2]. \end{aligned} \quad (3)$$

The parameter t_p represents the rms width of the pulses, C is the chirp parameter, t_0 is the unit interval of the train, and the symbols b_k are independent random variables describing their presence ($b_k = 1$) or absence ($b_k = 0$). The probability of presence will be denoted by p , so that the mean of each symbol is $\langle b_k \rangle = p$, and its standard deviation σ_b is $\sigma_b^2 = p(1 - p)$. Ideal conditions are recovered when $p = 1$. Unless stated otherwise, sums range from $-\infty$ to $+\infty$. To allow the possibility of repetition rates, the width of the individual pulses will be assumed to be shorter than the basic time slot, $t_p < t_0$. Using the kernel (2), the output-train envelope can be straightforwardly computed as

$$\begin{aligned} x_\xi(t) &= t_p(t_p^2 + C\xi - i\xi)^{-1/2} \sum_k b_k \\ &\times \exp[-(t - kt_0)^2(1 + iC)/2(t_p^2 + C\xi - i\xi)], \end{aligned} \quad (4)$$

resulting in a coherent superposition of dispersed pulses.

In Fig. 1, we present a simulation of the dispersion of a portion of a 10-GHz train ($t_0 = 100$ ps) randomly on-off keyed, after its pass through the first integer Talbot device, $\gamma/\alpha = 1$. The total dispersion of the device is $+1592$ ps²/rad. The probability of appearance of pulses in the train is $p = 0.5$. Pulses are unchirped and have a rms width of 12 ps. The ideal Talbot would reproduce the incoming train shifted by half a unit interval. The temporal spreading of pulses due to dispersion creates Talbot images formed by interference of pulses. This phenomenon is local, depending on the number of neighboring pulses around a given time slot. This leads to an unsat-

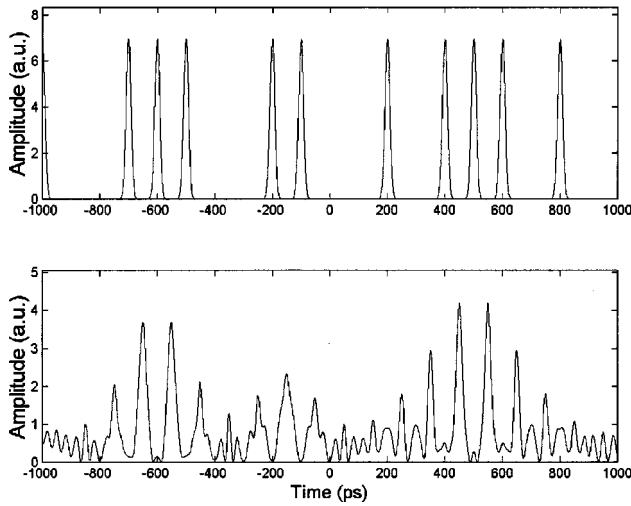


Fig. 1. Simulation of the form of the pulse envelope of 20-unit intervals of a 10-GHz, $p = 0.5$ random train of unchirped, 12-ps rms Gaussian pulses before (above) and after (below) its pass through a Talbot device with $\gamma/\alpha = 1$.

isfactory temporal signal, since the temporal characteristics of the output train depend on the local behavior of the input.

Nevertheless, wherever two pulses interfere in Fig. 1, they tend to form the desired ideal output train. Then, a spectral analysis of the signal can unveil the ability of the Talbot device to reconstruct output harmonics in a non-ideal situation. In the Fourier domain, the output $\hat{X}_\xi(\omega)$ train envelope is

$$\begin{aligned} \hat{X}_\xi(\omega) &= H_\xi(\omega)\hat{X}_0(\omega) \\ &= t_p \sqrt{\frac{2\pi}{1+iC}} \exp(-\rho\omega^2/2) \sum_k b_k \exp(-i\omega k t_0), \end{aligned} \quad (5)$$

where we have introduced the parameter

$$\rho = \frac{t_p^2}{1+C^2} - i\xi - i \frac{C t_p^2}{1+C^2}. \quad (6)$$

In formula (5), $H_\xi(\omega) = \exp(i\xi\omega^2/2)$ is the transfer function of kernel (2) and $\hat{X}_0(\omega)$ is the Fourier transform of input train (3). The basis of the Talbot effect is easily derived in the Fourier domain. For an exact periodic train of period t_0 , the spectral content of the input field consists of a set of delta functions at $\omega = 2\pi k/t_0$, with k an integer. For instance, when the Talbot device is an integer, $|\xi| = t_0^2\gamma/2\pi$, the transfer function for these frequencies reduces to $H_\xi(2\pi k/t_0) = \exp(i\pi\gamma k^2) = (-1)^{k\gamma}$. Then, the Talbot effect maintains the spectral components for γ even, and it adds a relative phase shift of π for γ odd. This phase shift is equivalent to a temporal shift of half a period in the time domain. Therefore the constructive interference of coherent adjacent pulses in Fig. 1, which provides intensity peaks between original pulses, is a consequence of the conservation of the relative harmonic content of the envelope by dispersion.

In Eq. (6), we notice that the initial chirp of the pulses can be absorbed in the definition of the total dispersion ξ

and the pulse width t_p . This means that chirping the pulses is a method of changing slightly the value of the total dispersion or that slight deviations of the dispersion from a design value can be interpreted as an additional chirping of the pulses and a change in its width, when the pulses are initially unchirped. However, if pulses are initially chirped, deviations of dispersion cannot be absorbed in the values of C and t_p . In the following sections, we analyze exact Talbot values, i.e., values of the form $|\xi| = t_0^2\gamma/2\pi\alpha$, retaining the parameter C as the true chirp of the pulses of the initial train. In any case, our formulas in this section are suitable for the analysis of deviations of the value of dispersion, since the approximations we derive assume only that the dispersion induced by the Talbot device, $|\xi| \sim t_0^2$, is larger than the last term in Eq. (6), which is in the worst case of the order of t_p^2 .

Since dispersion is a phase-only filter, the Talbot effect leaves the power spectrum $|\hat{X}_0(\omega)|^2$ of the optical envelope invariant. However, if detection occurs after the dispersive device, the generated photocurrent is proportional to the squared train envelope, $y_\xi(t) = |x_\xi(t)|^2$. Here we assume that the detection unit has a sufficiently large bandwidth to follow the train envelope. Detection is a nonlinear transformation of the stochastic variables $x_\xi(t)$ or $\hat{X}_\xi(\omega)$. Thus dispersion-induced phases causing pulse spreading can show now observable consequences.

The power spectrum of the detected train is computed by Fourier transforming the mean correlator²⁰:

$$\begin{aligned} S_\xi(\omega) &= \int_{-\infty}^{+\infty} d\tau \exp(-i\omega\tau) \\ &\times \left[\lim_{T \rightarrow \infty} \frac{1}{2T} \int_{-T}^T dt \langle y_\xi(t+\tau)y_\xi(t) \rangle \right], \end{aligned} \quad (7)$$

where the photocurrent correlator is

$$\begin{aligned} \langle y_\xi(t)y_\xi(t') \rangle &= \iint \frac{d\omega_1}{2\pi} \frac{d\omega_2}{2\pi} \exp[i(\omega_1 t - \omega_2 t')] \\ &\times \langle \hat{Y}_\xi(\omega_1)\hat{Y}_\xi(\omega_2)^* \rangle. \end{aligned} \quad (8)$$

The Fourier form of the photocurrent $\hat{Y}_\xi(\omega)$ is related to the Fourier form of the optical train envelope $\hat{X}_\xi(\omega)$ by an autocorrelation,

$$\begin{aligned} \hat{Y}_\xi(\omega) &= \int_{-\infty}^{+\infty} dt \exp(-i\omega t) y_\xi(t) \\ &= \int_{-\infty}^{+\infty} \frac{d\omega'}{2\pi} \hat{X}_\xi(\omega + \omega') \hat{X}_\xi(\omega')^*. \end{aligned} \quad (9)$$

Then, using Eq. (4), the Fourier form of the photocurrent can be expressed as

$$\hat{Y}_\xi(\omega) = \hat{F}(\omega) \sum_k B_k(\omega) \exp(-i\omega k t_0), \quad (10)$$

where $\hat{F}(\omega) = t_p \sqrt{\pi} \exp(-t_p^2\omega^2/4)$ is the Fourier transform of a single detected pulse, $|f(t)|^2$, and the functions $B_k(\omega)$ are

$$B_k(\omega) = b_k \sum_s b_{k-s} h_s(\omega) \exp(i\omega s t_0/2). \quad (11)$$

In this formula, the functions $h_s(\omega)$ are

$$\begin{aligned} h_s(\omega) &= \exp\left[\frac{C^2 t_p^2 \omega^2}{4(1+C^2)}\right] g_s(\omega) \\ &= \exp\left[\frac{C^2 t_p^2 \omega^2}{4(1+C^2)}\right] \\ &\quad \times \exp\left[-\frac{1+C^2}{4t_p^2}\left(\xi\omega + \frac{Ct_p^2\omega}{1+C^2} - st_0\right)^2\right], \end{aligned} \quad (12)$$

and they are peaked at $\omega = st_0 / [\xi + Ct_p^2/(1+C^2)]$. In Eq. (12), we have introduced the notation $g_s(\omega)$ for the second Gaussian function; this notation is used below.

To compute Eq. (7), let us suppose that the expected value at different frequencies of functions $B_k(\omega)$ is of the form

$$\begin{aligned} \langle B_k(\omega_1) B_m(\omega_2)^* \rangle &= \langle B_k(\omega_1) \rangle \langle B_m(\omega_2)^* \rangle \\ &\quad + \delta_{km} \Omega(\omega_1, \omega_2) + \Delta_{k-m}(\omega_1, \omega_2), \end{aligned} \quad (13)$$

where δ_{km} is the Kronecker delta, the asterisk denotes complex conjugation, and $\Omega(\omega_1, \omega_2)$ and $\Delta_{k-m}(\omega_1, \omega_2)$ are adimensional functions to be evaluated *a posteriori*. Then it is straightforward to show, using Eqs. (7)–(12), that the noise spectral density of the detected random train is related to this decomposition as

$$\begin{aligned} t_0 S_\xi^{(N)}(\omega) &= |\hat{F}(\omega)|^2 \\ &\quad \times \left[\Omega(\omega, \omega) + \sum_s \Delta_s(\omega, \omega) \exp(-i\omega st_0) \right]. \end{aligned} \quad (14)$$

Therefore only the diagonal values $\omega_1 = \omega_2 = \omega$ of the functions Ω and Δ_s are relevant. These adimensional functions can be computed from Eq. (11), using the following identity for the expected value of four-bit variables:

$$\begin{aligned} \langle b_i b_j b_k b_l \rangle &= p^4 + p^2 \sigma_b^2 \\ &\quad \times (\delta_{ij} + \delta_{ik} + \delta_{il} + \delta_{jk} + \delta_{jl} + \delta_{kl}) \\ &\quad + \sigma_b^2 a(p) (\delta_{ij} \delta_{jk} + \delta_{ij} \delta_{jl} + \delta_{ik} \delta_{kl} + \delta_{jk} \delta_{kl}) \\ &\quad + \sigma_b^4 (\delta_{ij} \delta_{kl} + \delta_{ik} \delta_{jl} + \delta_{il} \delta_{jk}) \\ &\quad + \sigma_b^2 b(p) \delta_{ij} \delta_{jk} \delta_{kl}, \end{aligned} \quad (15)$$

with $a(p) = p(1 - 2p)$ and $b(p) = 1 - 6p + 6p^2$. To check this formula, it suffices to consider all the different combinations of indices in both sides of the equality. Using Eq. (15), and after some algebra, the computation of the functions Ω and Δ_s yields

$$\begin{aligned} \Omega(\omega, \omega) &= \sigma_b^2 \left[p^2 |Z|^2 + 2ah_0(\omega) \text{Re}(Z) \right. \\ &\quad \left. + \sigma_b^2 \sum_s h_s^2(\omega) + bh_0^2(\omega) \right], \end{aligned} \quad (16)$$

$$\begin{aligned} \sum_s \Delta_s(\omega, \omega) \exp(-i\omega st_0) &= \sigma_b^2 \left[p^2 (Z^2 + |Z|^2 + Z^{*2}) + 2ah_0(\omega) \text{Re}(Z) \right. \\ &\quad \left. + \sigma_b^2 \sum_s h_s(\omega) h_{-s}(\omega) \right], \end{aligned} \quad (17)$$

where $Z(\omega) = \sum_s h_s(\omega) \exp(i\omega st_0/2)$, and Re stands for its real part. Finally, the power spectrum is

$$\begin{aligned} t_0 S_\xi^{(N)}(\omega) &= \sigma_b^2 |\hat{F}(\omega)|^2 \left\{ \left[h_0(\omega) + 2p \sum_{s>0} [h_s(\omega) \right. \right. \\ &\quad \left. \left. + h_{-s}(\omega)] \cos(\omega st_0/2) \right]^2 + \sigma_b^2 \sum_{s>0} [h_s(\omega) \right. \\ &\quad \left. + h_{-s}(\omega)]^2 \right\}. \end{aligned} \quad (18)$$

This formula contains the relevant filtering features of the random Talbot effect after detection. Our first task is to recover from Eq. (18) the noise power spectrum of the input train when it is detected before entering the Talbot device. This limit can be explored by setting $\xi = 0$ in the functions $h_s(\omega)$. The power spectrum is denoted by $S_0^{(N)}(\omega)$. In this situation, the value of the functions $h_s(\omega)$ is

$$h_s(\omega)_{\xi=0} = \exp\left(\frac{Ct_0\omega s}{2}\right) \exp\left[-(1+C^2)\frac{s^2 t_0^2}{4t_p^2}\right]. \quad (19)$$

Notice that, when $s = 0$, the value of these functions is unity, irrespective of the value of the frequency or the chirp. When $s \neq 0$, the value of these functions increases with positive or negative frequencies, depending on the relative signs of chirp and index s . The maximum value of the frequencies involved in Eq. (18) is determined by $\hat{F}(\omega)$, and it can be assumed that $|\omega|_{\max} = \kappa/t_p$ with, say, $\kappa \sim 10$. Then the leading contributions are of the form $\exp[|C|\kappa x - (1+C^2)x^2]$, with $x = |s|t_0/2t_p$, so that they are subleading with respect to unity if $x > \kappa$ or, equivalently, if $t_0/t_p > \kappa$. Since the period t_0 is assumed to be large compared with the pulse width t_p , the leading contribution of the functions $h_s(\omega)_{\xi=0}$ in Eq. (18) is due to the function with index $s = 0$. Then, $t_0 S_0^{(N)}(\omega) \cong \sigma_b^2 |\hat{F}(\omega)|^2$ in this approximation. This is the noise spectrum of a train of independent random pulses of the form $\sum_k b_k |f(t - kt_0)|^2$, as we expected. Notice that this limit can be recovered directly from Eqs. (10) and (11) since $B_k(\omega) \cong b_k^2 = b_k$ when $\xi = 0$. Notice also that the noise spectrum is broadband, and it follows the spectral density of a single detected pulse, $|\hat{F}(\omega)|^2$.

After the Talbot effect, Eq. (18) shows a different pattern, because of the new structure of $B_k(\omega)$. To analyze

the case $\xi \neq 0$, we derive a useful approximation to Eq. (18) that is used in the following. On one hand, we can factor out the first exponential in the expression of the functions $h_s(\omega)$ [see Eq. (12)], leaving the power spectrum in terms of the Gaussian functions $g_s(\omega)$. On the other hand, these Gaussian functions $g_i(\omega)$ with different indices have negligible overlapping, so that $g_i g_j \cong g_i^2 \delta_{ij}$. This can be checked directly from Eq. (12) by comparing the width of the Gaussian function with their separation. Since $t_p^2 \ll t_0^2 \approx |\xi|$, the separation between maxima of $g_s(\omega)$ and $g_{s+1}(\omega)$ is approximately $t_0/|\xi|$, while their width is $t_p/|\xi|$; thus their overlapping can be neglected.

With this approximation, the noise spectrum is

$$t_0 S_\xi^{(N)}(\omega) \cong \sigma_b^2 J(\omega) \left\{ g_0^2(\omega) + \sum_{s \neq 0} [4p^2 \cos^2(\omega s t_0/2) + \sigma_b^2] g_s^2(\omega) \right\}, \quad (20)$$

with $J(\omega) = \pi t_p^2 \exp[-t_p^2 \omega^2/2(1 + C^2)]$. Thus the spectrum after Talbot is a broadband envelope $J(\omega)$ multiplied by the term in brackets. When the initial pulses are unchirped, this broadband output noise-envelope function $J(\omega)$ is just the power spectrum of a single detected pulse, $|\hat{F}(\omega)|^2$, but for chirped pulses, the spectrum enhances its bandwidth. This enlargement is the same as the optical linewidth enhancement of the individual Gaussian pulses due to chirp, but here it appears as the noise envelope of the microwave power spectrum of the detected random train after the Talbot device.

The output noise spectral density, Eq. (18) or (20), depends therefore on all the parameters that describe the train: the probability of appearance of pulses (through p and σ_b^2), the parameters of the individual pulses (t_p and C), and the period of the train (t_0). On the contrary, the detection of the train before entering the dispersive device depends only on σ_b^2 and t_p . Notice that the dependence of the spectral content of $S_\xi^{(N)}(\omega)$ in Eqs. (18) and (20) with respect to the parameters that define the model varies continuously with the values of these parameters. In the next sections, we analyze the features of $S_\xi^{(N)}(\omega)$ in different regimes of the parameters.

3. ANALYSIS OF THE SPECTRAL WINDOWS

The first term of $S_\xi^{(N)}(\omega)$ in the sum in brackets in Eq. (20) is $g_0^2(\omega)$. This function gives contributions for small frequencies around the dc component in the microwave spectrum. The second term has a peaked structure due to the presence of a series of functions $g_s^2(\omega)$, each of them cosine-squared modulated by the factor $4p^2 \cos^2(\omega s t_0/2) + \sigma_b^2$. In this section, we consider a situation where variations in $g_s^2(\omega)$ dominate over the cosine modulation, so that this modulation can be approximated by a constant. Conditions for this limit are derived below. In our analysis on this limit, both the broadband output noise-envelope function $J(\omega)$ and the cosine modulation are assumed constant in the vicinity of the maxima of $g_s^2(\omega)$, yielding a local white-noise background. The basic property of the resulting spectrum is the fact that the

broadband noise envelope $\sigma_b^2 J(\omega)$ is filtered around each of the maxima of the functions $g_s^2(\omega)$, which we call spectral windows.

First we consider trains composed of unchirped pulses $C = 0$, so that the broadband input noise coincides with the broadband envelope in Eq. (19), $\sigma_b^2 J(\omega) = \sigma_b^2 |\hat{F}(\omega)|^2$. This broadband input noise survives around the maxima of the spectral windows $g_s^2(\omega)$, which are centered at $\omega = s t_0/|\xi| = s \alpha \omega_f/\gamma$, where the integer s is the window index. When the window index is a multiple of γ , $s = h \gamma$ for a certain integer h , the surviving frequency is a harmonic of the output train, h being the harmonic index. Between two consecutive output harmonics, there are $\gamma - 1$ different noise windows. Thus noise becomes narrowband around the harmonics and in definite locations between them. The 10-dB decay full width of these windows can be computed from the expression of $g_i(\omega)$, yielding a constant value for all the windows, $\Delta \omega = 4.3 \alpha \omega_f t_p / \gamma t_0$. Thus the spectral windows are narrower as the pulses are shorter and the dispersion is larger. Moreover, since the separation between consecutive spectral windows is also proportional to $\alpha \omega_f / \gamma$, the windows depend continuously on dispersion or Talbot index γ/α , much like the creases of an accordion. When dispersion is small, the accordion is open, so that windows are wider and more distant, and when dispersion is large, the accordion is closed, so that the windows are closer and their widths are smaller.

The peak value of noise in the top of these windows is raised above or lowered below the input noise envelope $\sigma_b^2 J(\omega) = \sigma_b^2 |\hat{F}(\omega)|^2$, depending on the factor $4p^2 + \sigma_b^2 = p(1 + 3p)$. The transition occurs for $p = 0.434$. For instance, for $p = 0.5$, the peak noise level in the top of the windows is raised 1 dB. Notice that both the window location and its width depend only on the dispersion of the

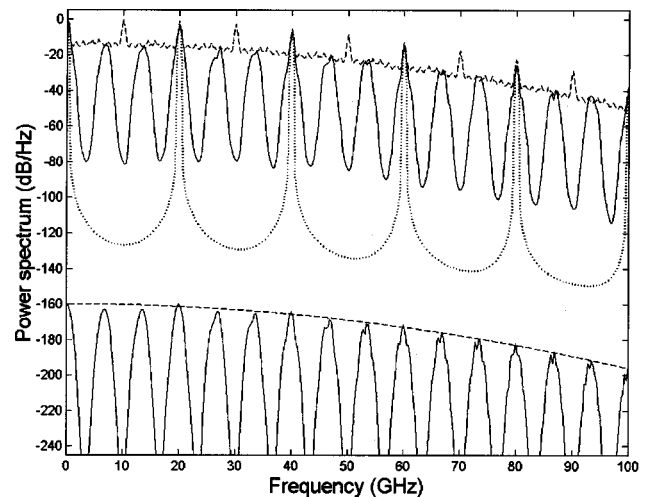


Fig. 2. Power spectrum of a detected 10-GHz, $p = 0.5$ random train of unchirped pulses with 6.5-ps rms width after its pass through a Talbot filter with $\gamma/\alpha = 3/2$. The upper part of the plot shows (continuous curve) the power spectrum of the detected output train, (dashed curve) the power spectrum of the detected input train, and (dotted curve) the mean signal power spectrum of both input and output trains. The lower part shows analytical approximations to the noise power spectrum: (continuous curve) output noise; (dashed curve) input noise.

device and the properties of the basic pulses, but the peak noise raising or lowering depends only on the parameter p .

This situation is illustrated in Fig. 2. We simulate a train of 300 pulses randomly distributed with $p = 0.5$. The pulse width is $t_p = 6.5$ ps, its chirp $C = 0$, and the frequency of the train is 10 GHz. The Talbot index is chosen as $\gamma/\alpha = 3/2$, corresponding to a total dispersion of $+2387$ ps²/rad. The exact Talbot replica would consist of a 20-GHz train. In the upper part of the plot, we present the input spectrum as a dashed curve and the output spectrum as a continuous curve. We also plot with dots the mean signal spectrum, consisting of a set of delta functions in the output harmonics. The finite width of these deltas is due to the finite dimensions of the simulated train. This part of the plot is normalized so that the peak value of the spectrum is 0 dB, and it allows visualization of the noise part of the spectral density. Below -160 dB, we present our approximation for the noise spectrum density, again with a dashed curve for the input train and with a continuous curve for the output train.

In Fig. 2, we observe that all spectral windows have the same width, $\Delta_{W\omega} = 1.83$ GHz. Noise survives around output harmonics and around multiples of 6.6 and 13.3 GHz. The raising of the peak noise level of the windows above the input noise level is, according to the above computation, 1 dB for $p = 0.5$. This value is imperceptible with the scales chosen in the figure. Finally, a certain small modulation can be observed in the higher spectral windows in the right part of the plot. The modulation is also present for low spectral windows not corresponding to output harmonics. For instance, the peak value in the 6.6-GHz spectral window is lowered with respect to the input noise due to nonmaximal modulation, i.e., the cosine-squared term maximum does not coincide with the top value of the window. The analysis of the modulation is treated in the next section.

Now we analyze the chirped case. The first difference is a shift in the centers of the spectral windows. From Eq. (12), they are located at

$$\begin{aligned} \omega &= \frac{st_0}{\left| \xi + \frac{Ct_p^2}{1+C^2} \right|} \\ &\cong \omega_f \frac{s\alpha}{\gamma} \left[1 - \text{sign}(\xi) \frac{\alpha}{\gamma} \frac{2\pi C}{1+C^2} \frac{t_p^2}{t_0^2} \right] \\ &= \omega_f \frac{s\alpha}{\gamma} + \Delta_{\text{peak}}^{(s)}\omega, \end{aligned} \quad (21)$$

where s is an arbitrary integer. Thus noise survives in the vicinity of multiples of a basic frequency. In the approximation of Eq. (21), we use again that the dispersion scale determined by $|\xi|$ is larger than t_p^2 , so that the denominator is $|\xi + Ct_p^2/(1+C^2)| = \text{sign}(\xi)[\xi + Ct_p^2/(1+C^2)]$. The centers of the spectral windows are shifted depending on the relative sign of chirp and dispersion. For instance, in positive-dispersion devices ($\xi > 0$), the center is redshifted (blueshifted) if the chirp is positive (negative). This shift is maximum when $C = \pm 1$ and

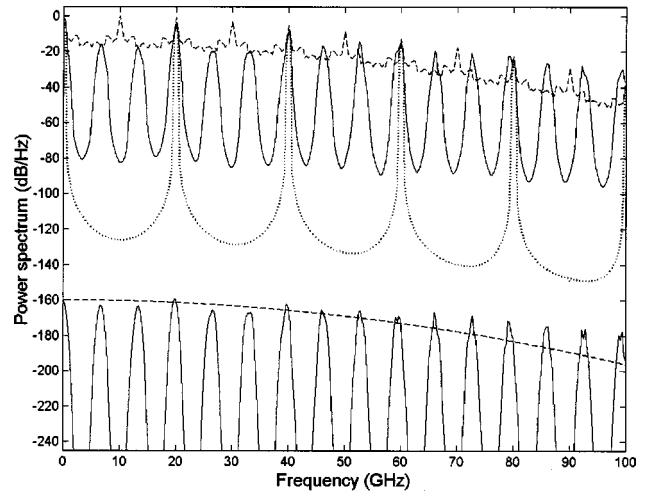


Fig. 3. Same as in Fig. 2, but with chirped pulses with $C = +1$.

represents a relative deviation of $\pi\alpha t_p^2/\gamma t_0^2$ with respect to the center of the unchirped value. The chirp-induced shift is therefore proportional to the value of the frequency in the spectral window center. In the last part of formula (21), we introduce the shift of the s spectral window, $\Delta_{\text{peak}}^{(s)}\omega$, used below.

The width of the spectral windows depends also on the chirp. From the form of the Gaussian functions $g_i(\omega)$, Eq. (12), it is easy to show that the 10-dB-decay full width decreases with the chirp parameter. The exact full width is

$$\begin{aligned} \Delta_{W\omega} &= 4.3 \frac{t_p}{\sqrt{1+C^2}} \left| \xi + \frac{Ct_p^2}{1+C^2} \right|^{-1} \\ &\cong 4.3\omega_f \frac{\alpha}{\gamma} \frac{t_p}{t_0} \frac{1}{\sqrt{1+C^2}}, \end{aligned} \quad (22)$$

where, in the last approximation, we assume again that $|\xi| \gg t_p^2$. Thus chirp reduces the width of the spectral windows irrespective of its sign. Finally, the peak noise level in the top of the spectral windows of a train of chirped pulses can be raised or lowered depending on the value of p , as in the unchirped case. But this peak noise level also suffers the bandwidth enlargement of the wideband output noise envelope, $J(\omega)$, which always raises the peak noise level over the initial broadband noise.

In Fig. 3, we present a simulation of a train composed of chirped pulses. The chirp parameter is chosen as $C = +1$. The remaining parameters are as in Fig. 2. The output noise envelope is broader than the input level owing to the existence of chirp. The spectral window width is $\Delta_{W\omega} = 1.32$ GHz, and the relative redshift of the centers is 8.85×10^{-3} . For instance, the fourth output harmonic at 80 GHz is redshifted 708 MHz. We see a modulation of high-order harmonics, as in Fig. 2, and the lowering of the noise peak level of spectral windows, corresponding to nonoutput harmonics in the left part of the plot, owing to nonmaximal modulation.

From relations (21) and (22), it is straightforward to realize that the magnitude and chirp of the individual

pulses can be extracted from the values of the spectral window width and the spectral windows shift. To be precise,

$$C = -2.9 \operatorname{sign}(\xi) \frac{\omega_f \Delta_{\text{peak}}^{(s)}}{s (\Delta_W \omega)^2}. \quad (23)$$

This measurement can be performed for any spectral window, not necessarily one of those surrounding the harmonics (s multiple of γ). Notice also that it is independent of the concrete Talbot device used, since it does not depend on the value of the Talbot index. This expression is also valid when modulation of the spectral windows is present, although in those cases a fitting of the whole spectral window can be necessary to obtain precise values of width and shift.

4. ANALYSIS OF THE MODULATION

The spectral windows $g_i(\omega)$ are modulated by a cosine-squared term both in the chirped and in the unchirped cases. Given a window index s , the maximum value of the modulation factor $4p^2 \cos^2(\omega s t_0/2) + \sigma_b^2$ occurs for

$$\omega = m \omega_f / s, \quad (24)$$

with m any integer. It is easy to show that in trains composed of unchirped pulses, the modulation and window maxima coincide for the output harmonics, and only in these cases. Therefore nonoutput harmonic windows ($s \neq h \gamma$) can show tips on top of the spectral windows, or lowering of the peak noise level if they are sufficiently narrow. When the pulses are chirped, the modulation maxima still remain over the harmonics, but the spectral windows are shifted.

The spectral modulation full width in the window of index s is

$$\Delta_M \omega = \omega_f / s. \quad (25)$$

In particular, the output harmonics correspond to indices $s = h \gamma$ so that $\Delta_M \omega = \omega_f / h \gamma$. This width becomes smaller as the harmonic or window index becomes larger, but it does not depend on the train characteristics, such as the temporal width, t_p , the value of the chirp, C , or the value of p . Then, modulation of the s spectral windows appears when $\Delta_M \omega < \Delta_W \omega$, or equivalently when

$$4.3 t_p > \frac{\gamma t_0}{\alpha s}. \quad (26)$$

Then, modulation is present when the spectral window index s is high, the dispersion γ/α is small, or the relative width of the pulses t_p/t_0 is high.

The limit described in relation (26) is exemplified in Fig. 4, where we simulate a random 10-GHz train composed of 400 pulses with $t_p = 10$ ps, $\gamma/\alpha = 1$, $\xi = +1592$ ps²/rad, and $p = 0.9$, so that the output train also has 10 GHz. The 10-dB window full width is 4.3 GHz, while the modulation width in output harmonics is $10/h$ GHz, so that modulation is expected to be observable after the third output harmonic. The conventions in this plot are as in the previous figures. The peak noise level is raised 5.2 dB owing to the simulation of a nearly full train with $p = 0.9$.

When modulation of a spectral window appears, the decay around the peak value has to consider both $\Delta_W \omega$ and $\Delta_M \omega$. However, since the modulation occurs for high harmonics, small dispersion, and broad pulses, the decay due to the structure of the spectral window is usually negligible, since $\Delta_W \omega$ is larger than $\Delta_M \omega$. Using relation (20), it is straightforward to compute the decay Γ between noise level in the harmonic and the first modulation zero due only to modulation, $\Gamma(\text{dB}) = 10 \log(1 + 3p)/(1 - p)$. In Fig. 4, the decay Γ is 16 dB. In the worst case ($p = 0.5$), Γ attains a minimum value of 7 dB. This is also the typical value of decay between consecutive maxima and minima of modulation in the same spectral window. When the approximation fails because $\Delta_W \omega$ and $\Delta_M \omega$ are of the same order, or when the center of the spectral win-

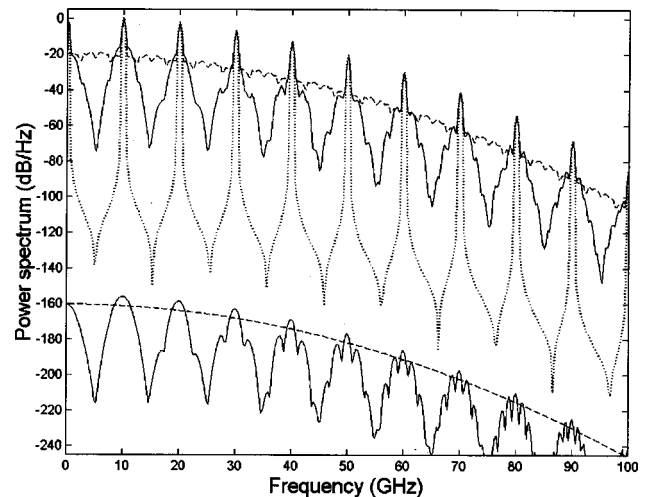


Fig. 4. Power spectrum of a detected 10-GHz, $p = 0.9$ random train of unchirped pulses with 10-ps rms width after its pass through a Talbot filter with $\gamma/\alpha = 1$. The upper part of the plot shows (continuous curve) the power spectrum of the detected output train, (dashed curve) the power spectrum of the detected input train, (dotted curve) the mean signal power spectrum of both input and output trains. The lower part shows analytical approximations to the noise power spectrum: (continuous curve) output noise; (dashed curve) input noise.

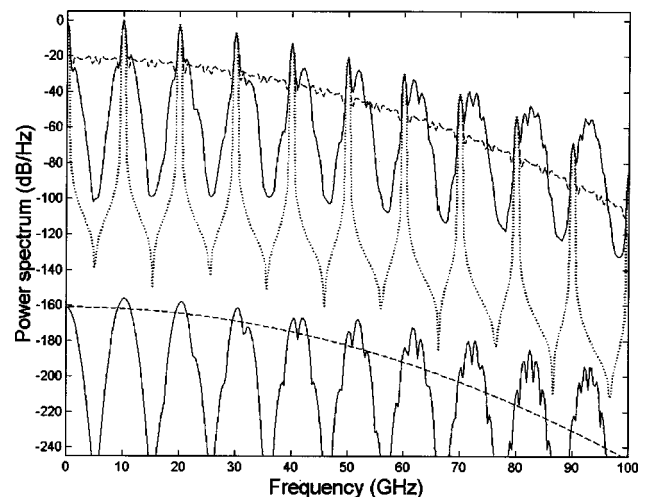


Fig. 5. Same as in Fig. 2, but with chirped pulses with $C = -1$.

dow is shifted owing to the chirp of the basic pulses, the value of the decay Γ has to be reevaluated from relation (20).

To complete our examples, in Fig. 5 we plot our final simulation where chirp is taken into account. We choose the same parameters of simulation as in Fig. 4, except the value of the chirp, whose value is $C = -1$. The chirped train blueshifts the center of the spectral windows, while the modulation does not change the position of its maxima. This results in asymmetric patterns of modulation. The other features of the spectrum are as in Fig. 4.

5. CONCLUSIONS

We have computed the exact power spectrum of a random and coherent train of pulses detected after its pass of a general Talbot device, and we have described its general characteristics. The technical assumptions in our derivation have been, first, the use of an ideal Talbot filter with enough bandwidth to cope with the optical bandwidth of the incoming train and to produce pure first-order dispersion; second, the absence of nonlinear effects or attenuation; third, the representation of pulses as linearly chirped and Gaussian; fourth, ideal detection; and finally, the independence of the bit variables describing the presence or absence of pulses.

As a consequence of the coherent interference of dispersed pulses, the microwave spectrum after the detection of the train has a broadband noise envelope that follows the linewidth spectrum of an individual pulse, i.e., the microwave envelope bandwidth is enhanced by the value of the chirp. The basic feature of the spectrum is the presence of spectral windows that act as filters of this broadband noise, whose centers are shifted with respect to the harmonics due to the chirp of the incident pulses. Measurement of the relative deviation of these centers with respect to spectral-window width allows a determination of the chirp's sign and magnitude. The width of the spectral windows is narrower as the dispersion of the device decreases, the pulse width is shorter, and the chirp is larger. The peak value of these windows depends on the relative amount of pulses in the train.

For small dispersion devices, high spectral windows, and wide pulses, the spectral windows show a cosine-squared modulation. The width of this modulation is a fraction of the input harmonic value, being independent of the relative amount of pulses in the train or of the properties of the pulses in the train.

In conclusion, our analysis shows that the parameters describing the pulse train have a neat influence in the resulting microwave spectrum, allowing the indirect characterization of pulse trains through the random Talbot effect. In experimental situations, however, the random Talbot effect has to coexist with other types of broadband and narrowband noise due to the sources or modulators used, such as amplitude noise or timing jitter. For instance, as is well known, the spectrum of detected pulse trains from mode-locked lasers show typical noise skirts around output harmonics, whose width depends on the correlation properties of noise (see, for instance, Refs. 21–23, and references therein). Moreover, deviations of the ideal behavior of the Talbot filter will also affect the char-

acteristics of the spectrum. Although it seems unlikely that the random Talbot effect of pulse trains shows all the fine spectral details contained in Eq. (18) or (20), the overall features should be still present. Despite this fact, the exact solution for the on-off keying noise spectral density presented here represents, to the best of our knowledge, the first study in the theoretical description of the noise features in Talbot devices, which can be enlarged when required by concrete experimental circumstances.

ACKNOWLEDGMENTS

This work has been supported by Ministerio de Ciencia y Tecnología, Spain, under contract TIC 2003-03041.

REFERENCES

1. T. Jansson and J. Jansson, "Temporal self-imaging effect in single-mode fibers," *J. Opt. Soc. Am.* **71**, 1373–1376 (1981).
2. I. Shake, H. Tahara, S. Kawanishi, and M. Saruwatari, "High-repetition-rate optical pulse generation by using chirped optical pulses," *Electron. Lett.* **34**, 792–793 (1998).
3. S. Arahira, S. Kutsuzawa, Y. Matsui, D. Kunimatsu, and Y. Ogawa, "Repetition-frequency multiplication of mode-locked pulses using fiber dispersion," *J. Lightwave Technol.* **16**, 405–410 (1998).
4. V. P. Minkovich, A. N. Starodumov, V. I. Borisov, V. I. Ledebev, and S. N. Perepechko, "Temporal interference of coherent laser pulses in optical fibers," *Opt. Commun.* **192**, 231–235 (2001).
5. J. Azaña and M. A. Muriel, "Technique for multiplying the repetition rates of periodic trains of pulses by means of a temporal self-imaging effect in chirped fiber gratings," *Opt. Lett.* **24**, 1672–1674 (1999).
6. S. Longhi, M. Marano, P. Laporta, O. Svelto, M. Belmonte, B. Agogliati, L. Arcangeli, V. Pruneri, M. N. Zervas, and M. Ibsen, "40-GHz pulse-train generation at 1.5 μm with a chirped fiber grating as a frequency multiplier," *Opt. Lett.* **25**, 1481–1483 (2000).
7. N. K. Berger, B. Vodonos, S. Atkins, V. Smulakovsky, A. Bekker, and B. Fischer, "Compression of periodic light pulses using all-optical repetition rate multiplication," *Opt. Commun.* **217**, 343–349 (2003).
8. M. Marano, S. Longhi, P. Laporta, M. Belmonte, and B. Agogliati, "All-optical square-pulse generation and multiplication at 1.5 μm by use of a novel class of fiber Bragg gratings," *Opt. Lett.* **26**, 1615–1617 (2001).
9. J. Azaña, P. Kockaert, R. Slavik, L. R. Chen, and S. LaRochelle, "Generation of a 100-GHz optical pulse train by pulse repetition-rate multiplication using superimposed fiber Bragg gratings," *IEEE Photon. Technol. Lett.* **15**, 413–415 (2003).
10. D. A. Chestnut, C. J. S. de Matos, and J. R. Taylor, "4x repetition-rate multiplication and Raman compression of pulses in the same optical fiber," *Opt. Lett.* **27**, 1262–1264 (2002).
11. S. Atkins and B. Fischer, "All-optical pulse rate multiplication using fractional Talbot effect and field-to-intensity conversion with cross-gain modulation," *IEEE Photon. Technol. Lett.* **15**, 132–134 (2003).
12. B. Fischer, B. Vodonos, S. Atkins, and A. Bekker, "Dispersion-mode pulsed laser," *Opt. Lett.* **25**, 728–730 (2000).
13. S. Atkins, B. Vodonos, A. Bekker, and B. Fischer, "Fractional dispersion modes in a pulsed fiber laser," *Opt. Commun.* **222**, 393–397 (2003).
14. A. Kalestynski and B. Smolinska, "Self-restoration of the autoidolon of defective periodic objects," *Opt. Acta* **25**, 125–134 (1978).
15. K. Patorski, "The self-imaging phenomenon and its applications," *Prog. Opt.* **27**, 3–74 (1989).
16. C. R. Fernández-Pousa, F. Mateos, L. Chantada, M. T. Flores-Arias, C. Bao, M. V. Pérez, and C. Gómez-Reino,

- “Random jitter smoothing by Talbot effect. I. Variance,” *J. Opt. Soc. Am. B* (to be published).
17. J. Azaña, “Temporal self-imaging effects for periodic optical pulse sequences of finite duration,” *J. Opt. Soc. Am. B* **20**, 83–90 (2003).
 18. A. Papoulis, “Pulse compression, fiber communications, and diffraction: a unified approach,” *J. Opt. Soc. Am. A* **11**, 3–13 (1994).
 19. G. P. Agrawal, *Nonlinear Fiber Optics*, 3rd ed. (Academic, Boston, 2001).
 20. A. Papoulis, *Probability, Random Variables and Stochastic Processes*, 2nd ed. (McGraw-Hill, New York, 1984).
 21. R. P. Scott, C. Langrock, and B. H. Kolner, “High-dynamic-range laser amplitude and phase noise measurement techniques,” *IEEE J. Sel. Top. Quantum Electron.* **7**, 641–655 (2001).
 22. F. Rana, H. L. T. Lee, R. J. Ram, M. E. Grein, L. A. Jiang, E. P. Ippen, and H. A. Haus, “Characterization of the noise and correlations in harmonically mode-locked-lasers,” *J. Opt. Soc. Am. B* **19**, 2609–2621 (2002).
 23. T. Yilmaz, C. M. Depriest, A. Braun, J. H. Abeles, and P. J. Delfyett, “Noise in fundamental and harmonic mode-locked semiconductor lasers: experiments and simulations,” *IEEE J. Quantum Electron.* **39**, 838–848 (2003).